

Moment Tensors: Decomposition and Visualization

Václav Vavryčuk*

Institute of Geophysics, Czech Academy of Sciences, Prague, Czech Republic

Synonyms

Dynamics and mechanics of faulting; Earthquake source observations; Focal mechanism; Seismic anisotropy; Theoretical seismology

Introduction

Elastic waves are generated by forces acting at the source and affected by the response of a medium to these forces. Mathematically, they are expressed using the representation theorem (Aki and Richards 2002, Eq. 2.41):

$$u_i(\mathbf{x}, t) = \int_{-\infty}^{\infty} \iiint_V f_k(\boldsymbol{\xi}, \tau) G_{ik}(\mathbf{x}, t; \boldsymbol{\xi}, \tau) d\tau dV(\boldsymbol{\xi}), \quad (1)$$

where $u_i = u_i(\mathbf{x}, t)$ is the observed displacement field, \mathbf{x} is the position vector of an observer, t is time, and Green's tensor $G_{ik} = G_{ik}(\mathbf{x}, t; \boldsymbol{\xi}, \tau)$ is the solution of the equation of motion for a point single force with time dependence of the Dirac delta function. The Green's tensor is defined as the i th component of the displacement produced by a force in the x_k direction and describes propagation effects on waves along a path from the source to a receiver. Vector $f_k = f_k(\boldsymbol{\xi}, \tau)$ is the density of the body forces acting at the source being a function of the position vector $\boldsymbol{\xi}$ and time τ at the source. The integration in Eq. 1 is over focal volume V and time τ . For simplicity, an infinite medium is assumed in Eq. 1.

Seismic waves generated at an earthquake source and propagating in the Earth have some specific properties. Firstly, the body forces associated with the earthquake source are not distributed in a volume but along a fault. Secondly, the earthquake source is not represented by single forces but rather by dipole forces. The dipole forces cause the two blocks at opposite sides of the fault to mutually move (Fig. 1a). They are described by moment tensor density $m_{kl} = m_{kl}(\boldsymbol{\xi}, \tau)$ defined along fault Σ (Fig. 1b). A substitution of single forces by dipole forces leads to modifying Eq. 1 as follows (Burridge and Knopoff 1964; Aki and Richards 2002, Eq. 3.20):

$$u_i(\mathbf{x}, t) = \int_{-\infty}^{\infty} \iint_{\Sigma} m_{kl}(\boldsymbol{\xi}, \tau) \frac{\partial}{\partial \xi_l} G_{ik}(\mathbf{x}, t; \boldsymbol{\xi}, \tau) d\tau d\Sigma(\boldsymbol{\xi}). \quad (2)$$

If the size of the fault is small with respect to distance between the source and the receiver, the representation theorem can be simplified by introducing the point source approximation:

*Email: vv@ig.cas.cz

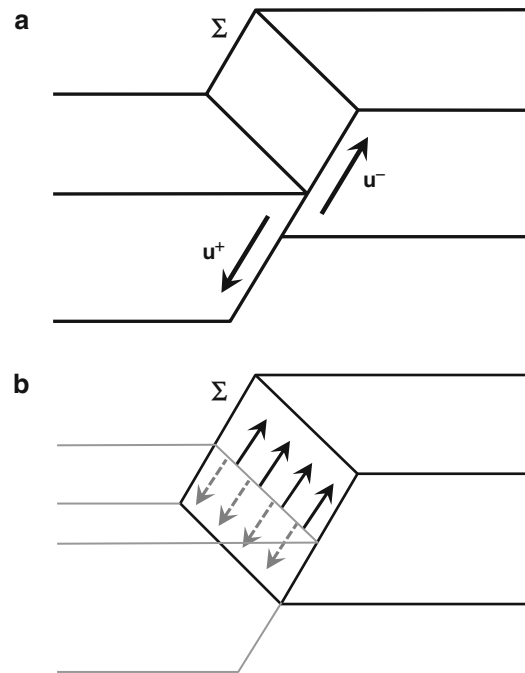


Fig. 1 (a) Example of motion (*normal faulting*) and (b) distribution of equivalent dipole forces along fault Σ

$$u_i(\mathbf{x}, t) = \int_{-\infty}^{\infty} M_{kl}(\tau) \frac{\partial}{\partial \xi_l} G_{ik}(\mathbf{x}, t; \boldsymbol{\xi}, \tau) d\tau, \quad (3)$$

or simply

$$u_i = M_{kl} * G_{ik,l}, \quad (4)$$

where $M_{kl} = M_{kl}(t)$ is the seismic moment tensor

$$M_{kl} = \iint_{\Sigma} m_{kl} d\Sigma, \quad (5)$$

and symbol “*” means the time convolution. Integration in Eq. 5 is performed over fault Σ . Moment tensor \mathbf{M} is a symmetric tensor describing nine couples of equivalent dipole forces which can act at the earthquakes source (Fig. 2). It is a basic quantity evaluated for earthquakes on all scales from acoustic emissions to large devastating earthquakes (see entries “► [Long-Period Moment-Tensor Inversion: The Global CMT Project](#),” “► [Reliable Moment Tensor Inversion for Regional- to Local-Distance Earthquakes](#),” and “► [Regional Moment Tensors Review: An Example from the Euro-Mediterranean Region](#)”).

The most common type of the moment tensor is the double-couple (DC) source which represents the force equivalent of shear faulting on a planar fault in isotropic media. However, many studies reveal that seismic sources often display more general moment tensors with significant non-double-couple (non-DC) components (Julian et al. 1998; Miller et al. 1998; see entry “► [Non-Double-Couple Earthquakes](#)”). An explosion is an obvious example of a non-DC source, but non-DC components can also be produced by a collapse of a cavity in mines (Rudajev and Šílený 1985), by inflation or deflation of magma chambers in

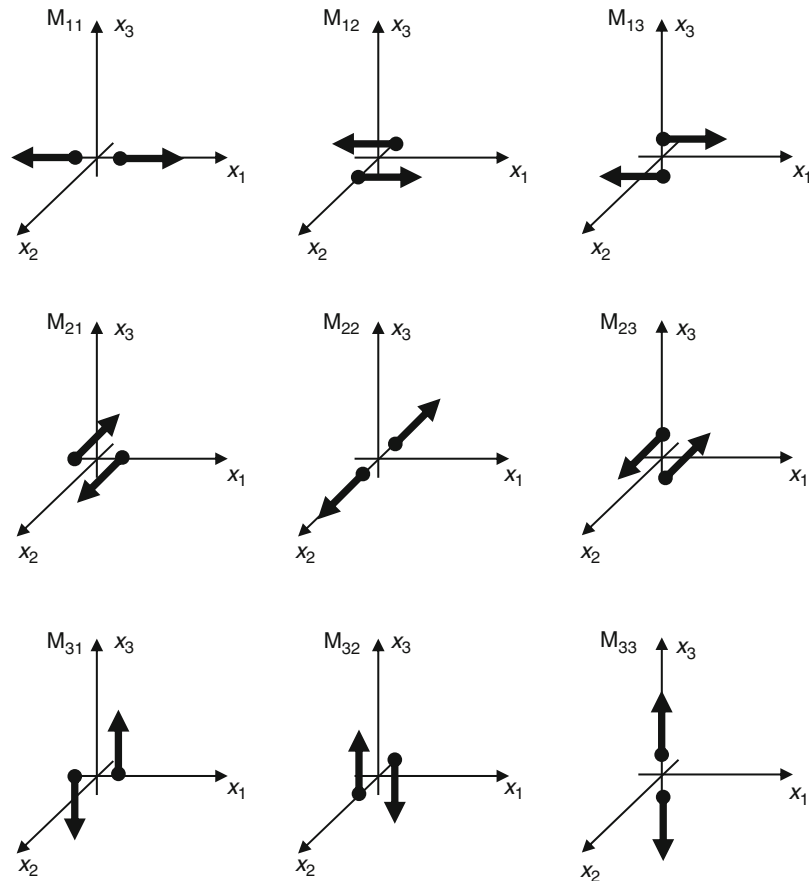


Fig. 2 Set of nine couples of equivalent dipole forces forming the moment tensor

volcanic areas (Mori and McKee 1987), by shear faulting on a nonplanar (curved or irregular) fault, by tensile faulting induced by fluid injection when the slip vector is inclined from the fault and causes its opening (Vavryčuk 2001, 2011), or by shear faulting in anisotropic media (Kawasaki and Tanimoto 1981; Vavryčuk 2005).

Moment Tensor Decomposition

In order to identify which type of seismic source is physically represented by a retrieved moment tensor \mathbf{M} , the moment tensor is usually diagonalized and decomposed into some elementary parts. The first step is the decomposition into its isotropic (ISO) and deviatoric (DEV) parts:

$$\mathbf{M} = \mathbf{M}_{\text{ISO}} + \mathbf{M}_{\text{DEV}}, \quad (6)$$

where

$$\mathbf{M}_{\text{ISO}} = \frac{1}{3} \text{Tr}(\mathbf{M}) \cdot \mathbf{I}, \quad (7)$$

and matrix \mathbf{I} is the identity matrix. The second step is the decomposition of the deviatoric part of \mathbf{M} . This step is more ambiguous and can be performed in many alternative ways. The deviatoric part can be

decomposed into three double couples (Jost and Herrmann 1989), into major and minor double couples (Kanamori and Given 1981; Wallace 1985), into double couples with the same T axis (Wallace 1985), or into a double couple and a compensated linear vector dipole (CLVD) component (Knopoff and Randall 1970). The last decomposition into the DC and CLVD components proved to be useful for physical interpretations and became widely accepted. This decomposition was further developed and applied by Sipkin (1986), Jost and Herrmann (1989), Kuge and Lay (1994), Vavryčuk (2015), and others, and it will be treated here in detail.

Definition of ISO, CLVD, and DC

The seismic moment tensor \mathbf{M} can be decomposed using eigenvalues and an orthonormal basis of eigenvectors in the following way:

$$\mathbf{M} = M_1 \mathbf{e}_1 \otimes \mathbf{e}_1 + M_2 \mathbf{e}_2 \otimes \mathbf{e}_2 + M_3 \mathbf{e}_3 \otimes \mathbf{e}_3, \quad (8)$$

where

$$M_1 \geq M_2 \geq M_3, \quad (9)$$

and vectors \mathbf{e}_1 , \mathbf{e}_2 , and \mathbf{e}_3 define the T (tension), N (intermediate or neutral), and P (pressure) axes, respectively. Symbol “ \otimes ” in Eq. 8 means the dyadic product of two vectors. Two basic properties of the moment tensor are separated in Eq. 8: (1) the orientation of the source defined by three eigenvectors and (2) the type and size of the source defined by three eigenvalues of \mathbf{M} . The eigenvalues can be represented as a point in three-dimensional (3-D) space (Riedesel and Jordan 1989):

$$\mathbf{m} = M_1 \hat{\mathbf{e}}_1 + M_2 \hat{\mathbf{e}}_2 + M_3 \hat{\mathbf{e}}_3, \quad (10)$$

where vectors $\hat{\mathbf{e}}_1$, $\hat{\mathbf{e}}_2$, and $\hat{\mathbf{e}}_3$ define the coordinate system in this space. In order to get a unique representation, the eigenvalues must be ordered according to Eq. 9. Consequently, the points representing the source type cannot cover the whole 3-D space but only its wedge called the “source-type space.” The choice of the coordinate system and the metric for parameterizing the source-type space differ for individual moment tensor decompositions.

For physical reasons, the three terms in Eq. 8 are further restructured to form isotropic (ISO), double-couple (DC), and compensated linear vector dipole (CLVD) parts (Fig. 3) in the following way (Knopoff and Randall 1970; Dziewonski et al. 1981; Sipkin 1986; Jost and Herrmann 1989):

$$\mathbf{M} = \mathbf{M}_{\text{ISO}} + \mathbf{M}_{\text{DC}} + \mathbf{M}_{\text{CLVD}} = M_{\text{ISO}} \mathbf{E}_{\text{ISO}} + M_{\text{DC}} \mathbf{E}_{\text{DC}} + M_{\text{CLVD}} \mathbf{E}_{\text{CLVD}}, \quad (11)$$

where \mathbf{E}_{ISO} , \mathbf{E}_{DC} , and \mathbf{E}_{CLVD} are the ISO, DC, and CLVD elementary (base) tensors and M_{ISO} , M_{DC} , and M_{CLVD} are the ISO, DC, and CLVD moments. The base tensors read

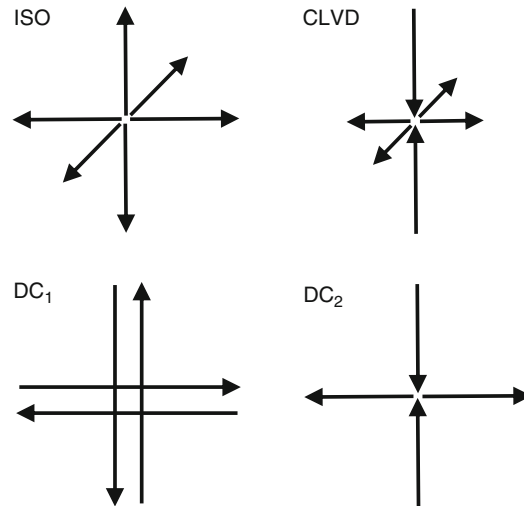


Fig. 3 The ISO, DC, and CLVD^- base tensors of the moment tensor. The DC part is plotted in the original coordinate system associated with the fault (DC_1) and after its diagonalization (DC_2)

$$\begin{aligned}
 \mathbf{E}_{\text{ISO}} &= \begin{bmatrix} 1 & 0 & 0 \\ 0 & 1 & 0 \\ 0 & 0 & 1 \end{bmatrix}, & \mathbf{E}_{\text{DC}} &= \begin{bmatrix} 1 & 0 & 0 \\ 0 & 0 & 0 \\ 0 & 0 & -1 \end{bmatrix}, \\
 \mathbf{E}_{\text{CLVD}}^+ &= \frac{1}{2} \begin{bmatrix} 2 & 0 & 0 \\ 0 & -1 & 0 \\ 0 & 0 & -1 \end{bmatrix}, & \mathbf{E}_{\text{CLVD}}^- &= \frac{1}{2} \begin{bmatrix} 1 & 0 & 0 \\ 0 & 1 & 0 \\ 0 & 0 & -2 \end{bmatrix},
 \end{aligned} \tag{12}$$

where $\mathbf{E}_{\text{CLVD}}^+$ or $\mathbf{E}_{\text{CLVD}}^-$ is used if $M_1 + M_3 - 2M_2 \geq 0$ or $M_1 + M_3 - 2M_2 < 0$, respectively. Hence, the CLVD tensor is aligned along the axis with the largest magnitude deviatoric eigenvalue. The eigenvalues of the base tensors are ordered according to Eq. 9 in order to lie in the source-type space. The norm of all base tensors, calculated as the largest magnitude eigenvalue (i.e., the maximum of $|M_i|$, $i = 1,2,3$), is equal to 1. This condition is called the unit “spectral norm” and physically means that the maximum dipole force of the base tensors is unity (Fig. 3). Alternative alignments of the CLVD tensor and other normalizations of the base tensors are also admissible (Chapman and Leaney 2012; Tape and Tape 2012) but have less straightforward physical interpretations.

Equations 11 and 12 uniquely define values M_{ISO} , M_{DC} , and M_{CLVD} expressed as follows:

$$M_{\text{ISO}} = \frac{1}{3}(M_1 + M_2 + M_3), \tag{13}$$

$$M_{\text{CLVD}} = \frac{2}{3}(M_1 + M_3 - 2M_2), \tag{14}$$

$$M_{\text{DC}} = \frac{1}{2}(M_1 - M_3 - |M_1 + M_3 - 2M_2|), \tag{15}$$

where M_{CLVD} includes also the sign of the elementary CLVD tensor. If the elementary CLVD tensor \mathbf{E}_{CLVD} is considered with its sign as in Eq. 11, then M_{CLVD} should be calculated as the absolute value of

Eq. 14. Values M_{ISO} , M_{DC} , and M_{CLVD} in Eqs. 13, 14, and 15 are usually further normalized and expressed using scalar seismic moment M and relative scale factors C_{ISO} , C_{DC} , and C_{CLVD} :

$$\begin{bmatrix} C_{\text{ISO}} \\ C_{\text{CLVD}} \\ C_{\text{DC}} \end{bmatrix} = \frac{1}{M} \begin{bmatrix} M_{\text{ISO}} \\ M_{\text{CLVD}} \\ M_{\text{DC}} \end{bmatrix}, \quad (16)$$

where M reads

$$M = |M_{\text{ISO}}| + |M_{\text{CLVD}}| + M_{\text{DC}}, \quad (17)$$

or equivalently (Bowers and Hudson 1999)

$$M = \|\mathbf{M}_{\text{ISO}}\| + \|\mathbf{M}_{\text{DEV}}\|, \quad (18)$$

where $\|\mathbf{M}_{\text{ISO}}\|$ and $\|\mathbf{M}_{\text{DEV}}\|$ are the spectral norms of the isotropic and deviatoric parts of moment tensor \mathbf{M} , respectively. Scale factors C_{ISO} , C_{DC} , and C_{CLVD} satisfy the following equation:

$$|C_{\text{ISO}}| + |C_{\text{CLVD}}| + C_{\text{DC}} = 1. \quad (19)$$

Equations 13, 14, 15, 16, and 17 imply that C_{DC} is always positive and in the range from 0 to 1; C_{CLVD} and C_{ISO} are in the range from -1 to 1. Consequently, the decomposition of \mathbf{M} can be expressed as

$$\mathbf{M} = M(C_{\text{ISO}} \mathbf{E}_{\text{ISO}} + C_{\text{DC}} \mathbf{E}_{\text{DC}} + |C_{\text{CLVD}}| \mathbf{E}_{\text{CLVD}}), \quad (20)$$

where M is the norm of \mathbf{M} calculated using Eq. 17 and represents a scalar seismic moment for a general seismic source. The absolute value of the CLVD term in Eq. 20 is used because the sign of CLVD is included in the elementary tensor \mathbf{E}_{CLVD} .

Physical Properties of the Decomposition

The above decomposition of the moment tensor is performed in order to physically interpret a set of nine dipole forces representing a general point seismic source and to identify easily some basic types of the source in isotropic media:

- The explosion/implosion is an isotropic source, and thus, it is characterized by $C_{\text{ISO}} = \pm 1$ and by zero C_{CLVD} and C_{DC} .
- Shear faulting is represented by the double-couple force and characterized by $C_{\text{DC}} = 1$ and by zero C_{ISO} and C_{CLVD} .
- Pure tensile or compressive faulting is free of shearing and thus characterized by zero C_{DC} . However, the non-DC components contain both ISO and CLVD. The ISO and CLVD components are of the same sign: they are positive for tensile faulting but negative for compressive faulting,
- Shear-tensile (dislocation) source defined as the source, which combines both shear and tensile faulting (Vavryčuk 2001, 2011), is characterized by nonzero ISO, CLVD, and DC components. The positive values of C_{ISO} and C_{CLVD} correspond to tensile mechanisms when fault is opening during rupturing. The negative values of C_{ISO} and C_{CLVD} correspond to compressive mechanisms when a fault is closing during rupturing. The ratio between non-DC and DC components defines the angle between the slip and the fault.

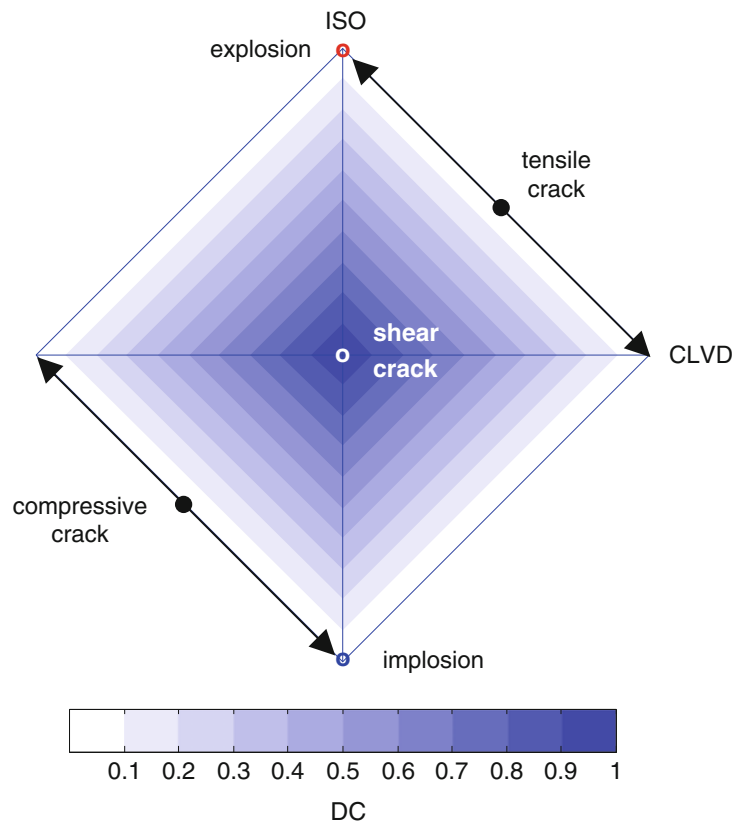


Fig. 4 Diamond CLVD-ISO source-type plot with positions of basic types of seismic sources. The *arrows* indicate the range of possible positions of moment tensors for pure tensile or compressive cracks

- Shear faulting on a nonplanar fault is characterized generally by a nonzero C_{DC} and C_{CLVD} . The C_{ISO} is zero, because no volumetric changes are associated with this type of source.

Source-Type Plots

For physical interpretations, it is advantageous to visualize the retrieved moment tensors graphically. Double-couple components of moment tensors are displayed using the well-known “beach balls” which show orientations of the fault together with the slip vector defining the shear motion along the fault (see entry “► [Earthquake Mechanism Description and Inversion](#)”). The non-double-couple components of moment tensors are displayed in the so-called source-type plots.

All moment tensors fill a source-type space which is a wedge in the full 3-D space. The magnitude of the vector in this space is the scalar moment, and its direction defines the type of the source. In order to identify the type of the source visually, it is convenient to plot all unit vectors of the source-type space in a 2-D figure using some projections. Here, three basic plots are mentioned: diamond CLVD-ISO plot (Vavryčuk 2015), Hudson’s skewed diamond plot (Hudson et al. 1989), and the Riedesel-Jordan lune plot (Riedesel and Jordan 1989).

Diamond CLVD-ISO Plot

The diamond CLVD-ISO plot shows the position of the source in the CLVD-ISO coordinate system in which the DC component is represented by the color intensity (Fig. 4). Since the sum of absolute values of

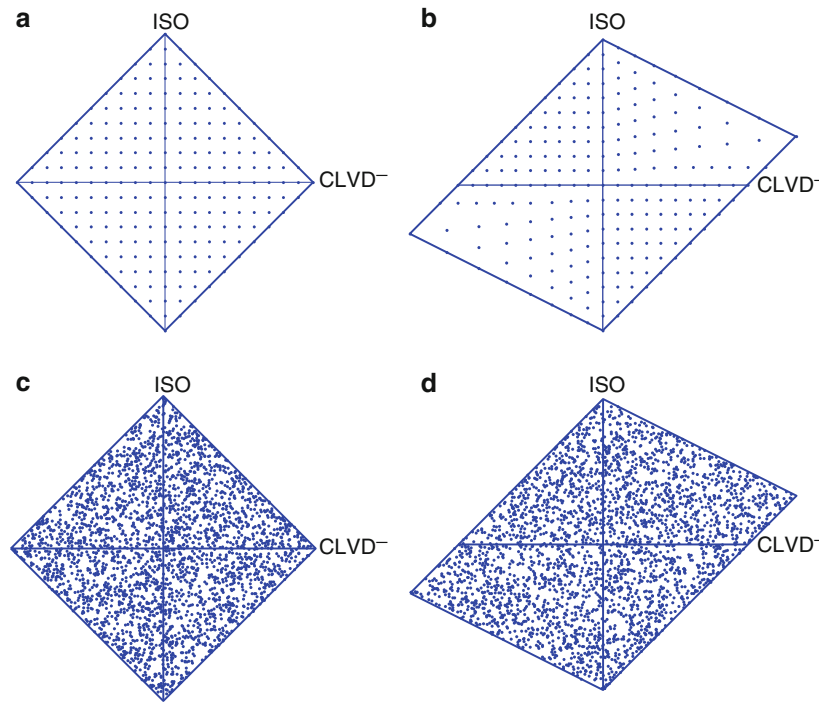


Fig. 5 The Hudson's diamond τ - k plot (a, c) and the skewed diamond u - v plot (b, d). The $CLVD^-$ means the reversed CLVD axis. The *dots* in (a, b) show a regular grid in C_{ISO} and C_{CLVD} from -1 to $+1$ with step of 0.1 . The *dots* in (c, d) show 3,000 sources defined by moment tensors with randomly generated eigenvalues. For scaling of the eigenvalues, see the text. Plots (c) and (d) indicate that the distribution of random sources is uniform in both projections

the CLVD and ISO cannot exceed 1, moment tensors must lie inside a diamond. A source with pure or predominant shear faulting is located at the origin of coordinates or close to it. An explosion or implosion source is located at the top or bottom vertex of the diamond, respectively. Motion on a pure tensile or compressive crack is plotted at the margin of the diamond. Points along the CLVD axis correspond to faulting on nonplanar faults, and points in the first and third quadrants of the diamond correspond to shear-tensile sources.

For pure tensile and shear-tensile sources, the ISO/CLVD ratio depends on the elastic properties of the medium surrounding the source. In isotropic media, this ratio is (Vavryčuk 2001, 2011)

$$\frac{C_{ISO}}{C_{CLVD}} = \frac{3}{4} \left(\frac{v_P}{v_S} \right)^2 - 1. \quad (21)$$

Hence, the point representing the pure tensile faulting in Fig. 4 (black dot) can be close to $C_{ISO} = 1$ (corresponding to an explosion) for high values of v_P/v_S but also close to $C_{CLVD} = 1$ for low values of v_P/v_S . The limiting cases are

$$\frac{v_P}{v_S} \rightarrow \infty \text{ and } \frac{v_P}{v_S} = \frac{2}{\sqrt{3}}, \quad (22)$$

describing fluids and the lower limit of stable solids ($\lambda = -2/3 \mu$), respectively. Similar conclusions can be drawn for pure compressive faulting (see Fig. 4).

Note that the abovementioned basic types of sources cannot be located in the second or fourth quadrants of the diamond source-type plot in Fig. 4. Moment tensors located in this area indicate

numerical errors of the moment tensor inversion, a more complicated source model or faulting in anisotropic media.

As mentioned above, values $C_{\text{ISO}} = \pm 1$ and $C_{\text{DC}} = 1$ correspond to an explosion/implosion and to shear faulting in isotropic media, respectively. Their physical meaning is thus straightforward. However, the moment tensor with $C_{\text{CLVD}} = 1$ does not correspond to any simple seismic source, and the presence of CLVD in moment tensors often causes confusions and poses questions whether it is necessary to introduce the CLVD. The decomposition described above indicates that the CLVD component is required to render the decomposition mathematically complete, and the CLVD component cannot thus be avoided. Although, it has no physical meaning itself, it can be interpreted physically in combination with the ISO component as a product of tensile faulting. In the case of a pure tensile crack, the CLVD component's major dipole is aligned with the normal to the crack surface and the volume change associated with the opening crack is described by the ISO component.

Hudson's Skewed Diamond Plot

Hudson et al. (1989) introduced two source-type plots: a diamond τ - k plot which is the diamond CLVD-ISO plot described in the previous section but with the opposite direction of the CLVD axis (Fig. 5a) and a skewed diamond u - v plot (Fig. 5b). The latter plot is introduced in order to conserve the uniform probability of moment tensor eigenvalues. If eigenvalues M_1 , M_2 , and M_3 have a uniform probability distribution between -1 and $+1$ and satisfy the ordering condition (9), then all points fill uniformly the skewed diamond plot. Axis u defines the deviatoric sources and axis v connects the pure explosive and implosive sources.

The moment tensor with arbitrary (but ordered) eigenvalues M_1 , M_2 , and M_3 is projected into the u - v plot using the following equations:

$$u = -\frac{2}{3M}(M_1 + M_3 - 2M_2), \quad v = \frac{1}{3M}(M_1 + M_2 + M_3), \quad (23)$$

where M is the scalar seismic moment calculated as the spectral norm of complete moment tensor \mathbf{M}

$$M = \max(|M_1|, |M_2|, |M_3|). \quad (24)$$

Equation 23 is similar to Eqs. 13 and 14 in the ISO-CLVD-DC decomposition except for scaling.

Figure 5a, b show mapping of a regular grid in C_{ISO} and C_{CLVD} calculated using Eqs. 13, 14, 15, 16, and 17 into the diamond CLVD-ISO plot and into the skewed diamond u - v plot. Figure 5b shows that the CLVD-ISO grid is deformed in the first and third quadrants of the u - v plot. Figure 5c, d demonstrate that sources with randomly generated eigenvalues cover uniformly the source-type plots. The uniform probability distribution function (PDF) is produced by the Hudson's skewed diamond plot (Fig. 5d) but also for the diamond CLVD-ISO plot. In this respect, the Hudson's skewed diamond plot does not provide any particular advantage compared to the standard CLVD-ISO plot (for details, see Tape and Tape 2012; Vavryčuk 2015).

Riedesel-Jordan Plot

A completely different approach is suggested by Riedesel and Jordan (1989) who introduce a compact plot displaying both the orientation and type of source on the focal sphere. Apparently, this plot looks simple and mathematically elegant but introduces difficulties. The moment tensor is represented by a vector defined in Eq. 10, and the coordinate axes $\hat{\mathbf{e}}_1$, $\hat{\mathbf{e}}_2$, and $\hat{\mathbf{e}}_3$ are identified with the T , N , and P axes of \mathbf{M} : \mathbf{e}_1 , \mathbf{e}_2 , and \mathbf{e}_3 defined in Eq. 8. The vector is normalized using the Euclidean norm

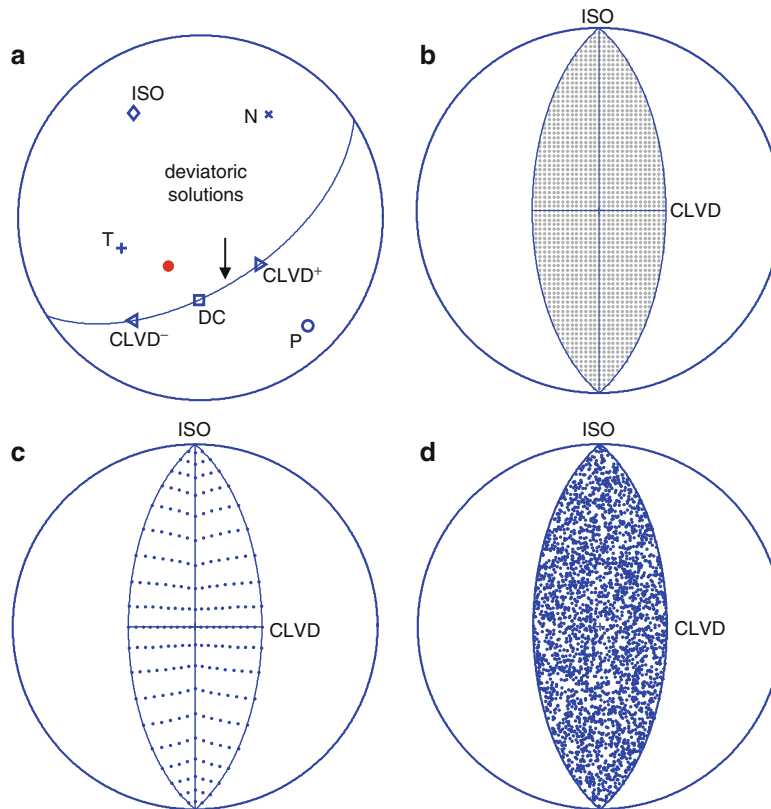


Fig. 6 Riedesel-Jordan source-type plot. **(a)** The original compact plot proposed by Riedesel and Jordan (1989) displaying the orientation of the moment tensor eigenvectors (P , T , and N axes), basic source types (ISO, CLVD, DC), and the position of the studied moment tensor (*red dot*). **(b, c, d)** A modified Riedesel-Jordan plot proposed by Chapman and Leaney (2012). The *dashed area* in **(b)** shows the area of admissible positions of sources. The *dots* in **(c)** show a regular grid in C_{ISO} and C_{CLVD} from -1 to $+1$ with step of 0.1 . The *dots* in **(d)** show 3,000 sources defined by moment tensors with randomly generated eigenvalues. Plot **(d)** indicates that the distribution of random sources is uniform in this projection

$$M = \sqrt{\frac{1}{2} (M_1^2 + M_2^2 + M_3^2)} \quad (25)$$

and projected on the sphere using a lower-hemisphere equal-area projection (see Fig. 6a).

Chapman and Leaney (2012) pointed out, however, that this representation is not optimum for several reasons. Firstly, vector \mathbf{m} cannot lie everywhere on the focal sphere but inside its small part called the “lune” (Tape and Tape 2012). The lune covers only one sixth of the whole sphere (see Fig. 6b). Secondly, vectors characterizing positive and negative isotropic sources (explosion and implosion) are physically quite different, but they are displayed in the same area on the focal sphere in this projection. Thirdly, analysis of uncertainties of a moment tensor solution by plotting a cluster of vectors \mathbf{m} includes both effects – uncertainties in the orientation and in the source type. This is fine if the moment tensor is nondegenerate. However, difficulties arise when the moment tensor is degenerate or nearly degenerate, because small perturbations cause significant changes of eigenvectors.

Some of the mentioned difficulties can be avoided by fixing the eigenvectors and analyzing the size of clusters produced by a varying source type only. If we fix the eigenvectors in the form

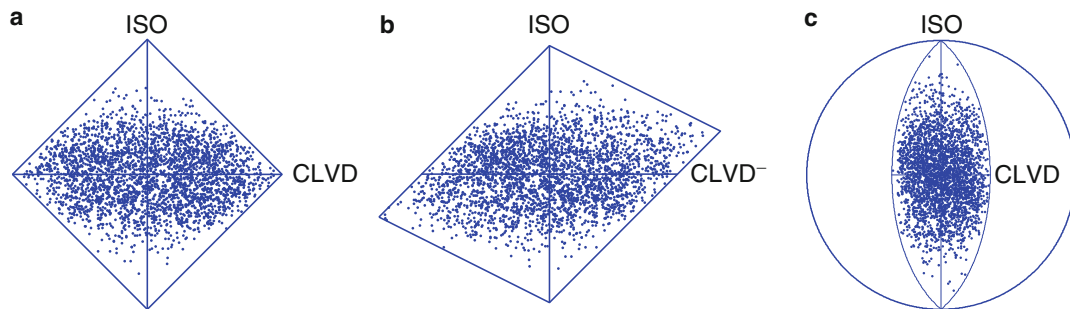


Fig. 7 Distribution of random sources displayed in three different source-type plots. **(a)** The diamond CLVD-ISO plot, **(b)** the Hudson's skewed diamond plot, and **(c)** the Riedesel-Jordan plot. The *dots* show 3,000 sources defined by moment tensors with randomly generated components in the interval from -1 to $+1$. The distribution of sources is nonuniform for all three source-type plots

$$\mathbf{e}_1 = \left(\frac{1}{\sqrt{3}}, \frac{1}{\sqrt{6}}, \frac{1}{\sqrt{2}} \right)^T, \mathbf{e}_2 = \left(\frac{1}{\sqrt{3}}, -\frac{2}{\sqrt{6}}, 0 \right)^T, \mathbf{e}_3 = \left(\frac{1}{\sqrt{3}}, \frac{1}{\sqrt{6}}, -\frac{1}{\sqrt{2}} \right)^T, \quad (26)$$

in the north-east-down coordinate system, we obtain a plot shown in Fig. 6b. This plot resembles the diamond CLVD-ISO plot (Fig. 4) but adapted to a spherical metric. The basic source types are characterized by the following unit vectors:

$$\mathbf{e}_{\text{ISO}} = \frac{1}{\sqrt{3}}(\mathbf{e}_1 + \mathbf{e}_2 + \mathbf{e}_3) = (1, 0, 0)^T, \quad (27)$$

$$\mathbf{e}_{\text{DC}} = \frac{1}{\sqrt{2}}(\mathbf{e}_1 - \mathbf{e}_3) = (0, 0, 1)^T, \quad (28)$$

$$\mathbf{e}_{\text{CLVD}}^+ = \sqrt{\frac{2}{3}} \left(\mathbf{e}_1 - \frac{1}{2}\mathbf{e}_2 - \frac{1}{2}\mathbf{e}_3 \right) = \left(0, \frac{1}{2}, \frac{\sqrt{3}}{2} \right)^T, \quad (29)$$

$$\mathbf{e}_{\text{CLVD}}^- = \sqrt{\frac{2}{3}} \left(\frac{1}{2}\mathbf{e}_1 + \frac{1}{2}\mathbf{e}_2 - \mathbf{e}_3 \right) = \left(0, -\frac{1}{2}, \frac{\sqrt{3}}{2} \right)^T. \quad (30)$$

Basic properties of the Riedesel-Jordan projection are exemplified in Fig. 6c, d. Figure 6c shows mapping of a regular grid in C_{ISO} and C_{CLVD} calculated using Eqs. 13, 14, 15, 16, and 17, and Fig. 6d indicates that the PDF of sources with randomly distributed eigenvalues M_1 , M_2 , and M_3 is uniform. For a detailed analysis on the probability of eigenvalues in the spherical projection, see Tape and Tape (2012).

Analysis of Moment Tensor Uncertainties Using Source-Type Plots

The source-type plots are often used for assessing uncertainties of the ISO, CLVD, and DC components of moment tensors. The reason for using the source-type plots for assessing the errors is simple. The moment tensor is usually plotted as a cluster of acceptable solutions, and the size of the cluster reflects uncertainties of the solution. Such approach is, however, simplistic and rough because the same uncertainties produce differently large clusters in dependence of the position of the cluster. Although the source-type plots

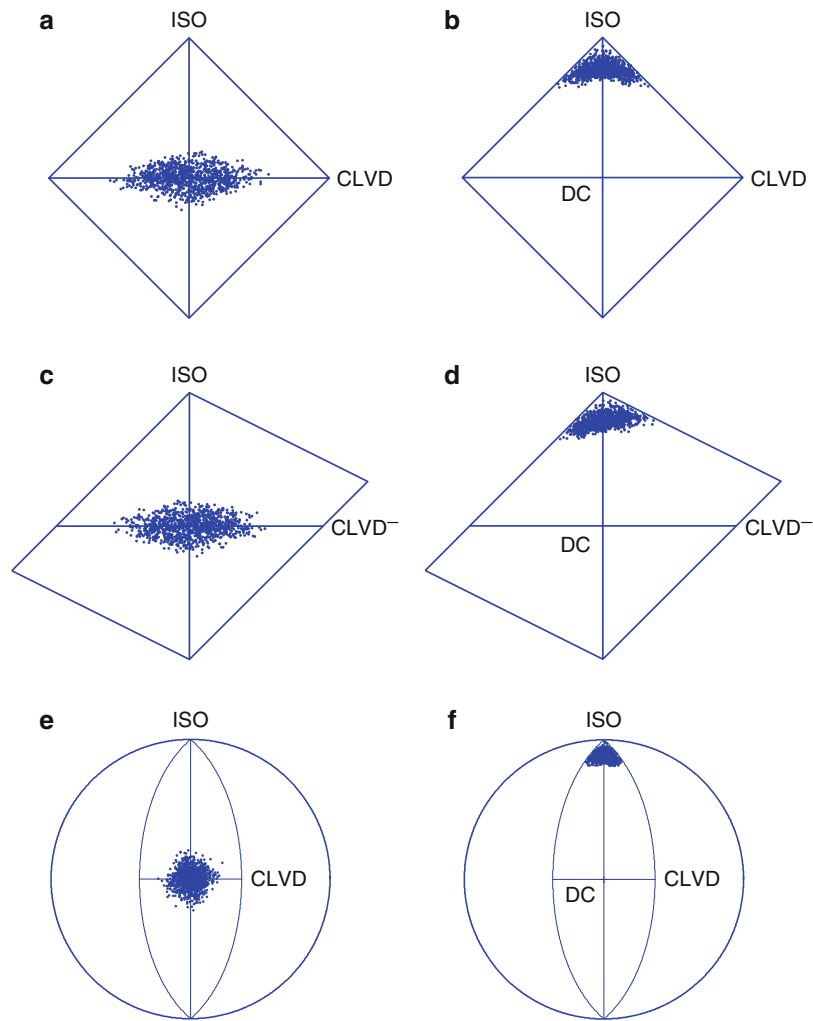


Fig. 8 Distribution of pure DC (*left-hand plots*) and pure explosive (*right-hand plots*) sources contaminated by random noise and displayed in three different source-type plots. (**a, b**) The diamond CLVD-ISO plot, (**c, d**) the Hudson's skewed diamond plot, and (**e, f**) the Riedesel-Jordan plot. The *dots* show 1,000 DC sources defined by the elementary tensor \mathbf{E}_{DC} (see Eq. (12)) and contaminated by noise with a uniform distribution from -0.25 to $+0.25$. The noise is superimposed to all tensor components

display a uniform PDF for randomly generated eigenvalues (see section “[Source-Type Plots](#)”), the behavior of moment tensor uncertainties is not simple. When uncertainties of moment tensor components are analyzed, the moment tensor is not in the diagonal form. After diagonalizing the moment tensor, the errors are projected into the errors of eigenvalues in a rather complicated way. This is demonstrated in Fig. 7. Moment tensors in this figure have all components random and distributed with a uniform probability in the interval from -1 to 1 . Nevertheless, some source types are quite rare. In particular, sources with a high explosive or implosive component are almost missing. This observation is common for all source-type plots.

More realistic sources are modeled in Fig. 8: the pure DC and ISO sources defined by tensors \mathbf{E}_{DC} and \mathbf{E}_{ISO} from Eq. 12 are contaminated by random noise with a uniform distribution in the interval from -0.25 to 0.25 . The noise is superimposed to all tensor components and 1,000 random moment tensors are generated. As expected, the randomly generated source tensors form clusters, but their shape is different for different projections and their size depends also on the type of the source. For the DC source (Fig. 8, left-hand plots), the maximum PDF is in the center of the cluster which coincides with the position of the

uncontaminated source. In the diamond CLVD-ISO plot and in the skewed diamond plot, the cluster is asymmetric being stretched along the CLVD axis. A more symmetric shape of the cluster is produced in the Riedesel-Jordan plot. However, the symmetry of the cluster is apparent because the CLVD and ISO axes are of different lengths. A significantly higher scatter of the CLVD components compared to the ISO components in moment tensor inversions has been observed and discussed also in Vavryčuk (2011). For the pure ISO source (Fig. 8, right-hand plots), the clusters are smaller than for the DC source, and the maximum PDF is out of the position of the uncontaminated source. This means that the ISO percentage is systematically underestimated due to errors of the inversion for highly explosive or implosive sources.

Source Tensor Decomposition

A simple classification of sources based on the moment tensor decomposition is possible in isotropic media only. In anisotropic media, the problem is more complicated. The moment tensor is affected not only by the geometry of faulting but also by the elastic properties of the focal zone. Depending on these properties, the moment tensors can take a general form with nonzero DC, CLVD, and ISO components even for simple shear faulting on a planar fault (Vavryčuk 2005). For this reason, physical interpretations of shear or tensile dislocation sources in anisotropic media should be based on the decomposition of the source tensor, which is directly related to geometry of faulting.

The source tensor \mathbf{D} (also called the potency tensor) is a symmetric dyadic tensor defined as (Ben-Zion 2003; Vavryčuk 2005)

$$D_{kl} = \frac{uS}{2}(s_k n_l + s_l n_k), \quad (31)$$

where vectors \mathbf{n} and \mathbf{s} denote the fault normal and the direction of the slip vector, respectively, u is the slip and S is the fault size. The relation between the source and moment tensors reads in anisotropic media (Vavryčuk 2005, his Eq. 4)

$$M_{ij} = c_{ijkl} D_{kl}, \quad (32)$$

and in isotropic media

$$M_{ij} = \lambda D_{kk} \delta_{ij} + 2\mu D_{ij}, \quad (33)$$

where c_{ijkl} is the tensor of elastic parameters and λ and μ are the Lamé's parameters. While the moment and source tensors diagonalize in anisotropic media in different systems of eigenvectors and thus their relation is complicated, the eigenvectors of the moment and source tensors are the same in isotropic media and their decomposition according to formulas in section "Definition of ISO, CLVD, and DC" yields similar results.

Properties of the moment and source tensor decompositions for shear and tensile sources in isotropic and anisotropic media are illustrated in Figs. 9 and 10. Figure 9 shows the source-type plots for tensile sources with a variable slope angle (i.e., the deviation of the slip vector from the fault) situated in an isotropic medium. The plot shows that the ISO and CLVD components are linearly dependent for both moment and source tensors. For the moment tensors, the line direction depends on the v_p/v_s ratio (Fig. 9a). For the source tensors, the line is independent of the properties of the elastic medium, and the C_{ISO}/C_{CLVD} ratio is always 1/2 (Fig. 9b). The differences between the behavior of the source and moment tensors are even more visible in anisotropic media. Figure 10 indicates that the ISO and CLVD components of the

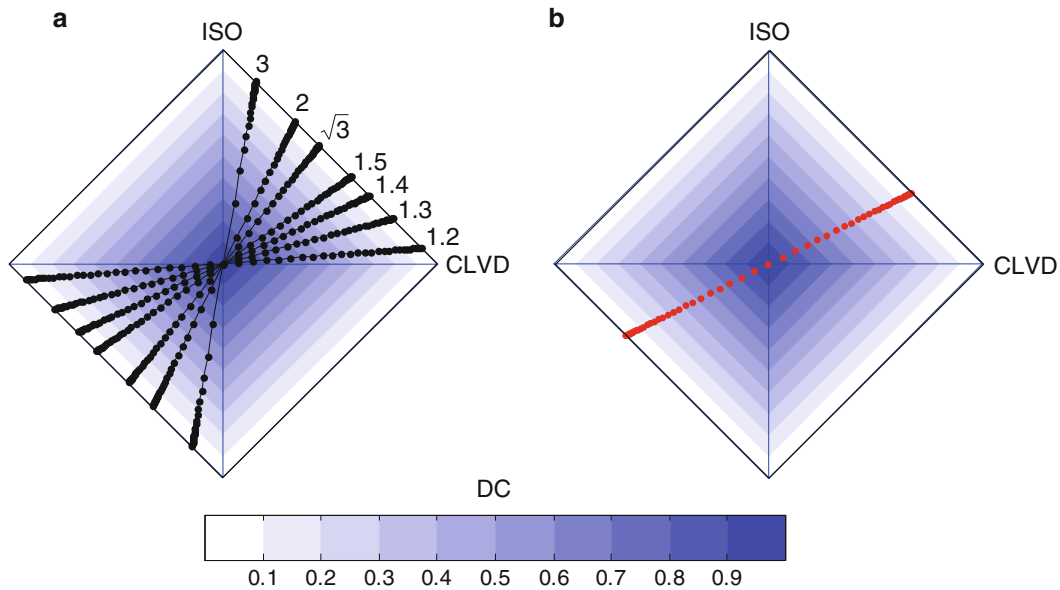


Fig. 9 Diamond source-type plots for the shear-tensile source model in an isotropic medium characterized by various values of the v_p/v_s ratios (the values are indicated in the plot). *Red dots*, source tensors; *black dots*, moment tensors. The *dots* correspond to the individual sources. The slope angle (i.e., the deviation of the slip vector from the fault) ranges from -90° (pure compressive crack) to $+90^\circ$ (pure tensile crack) in steps of 3°

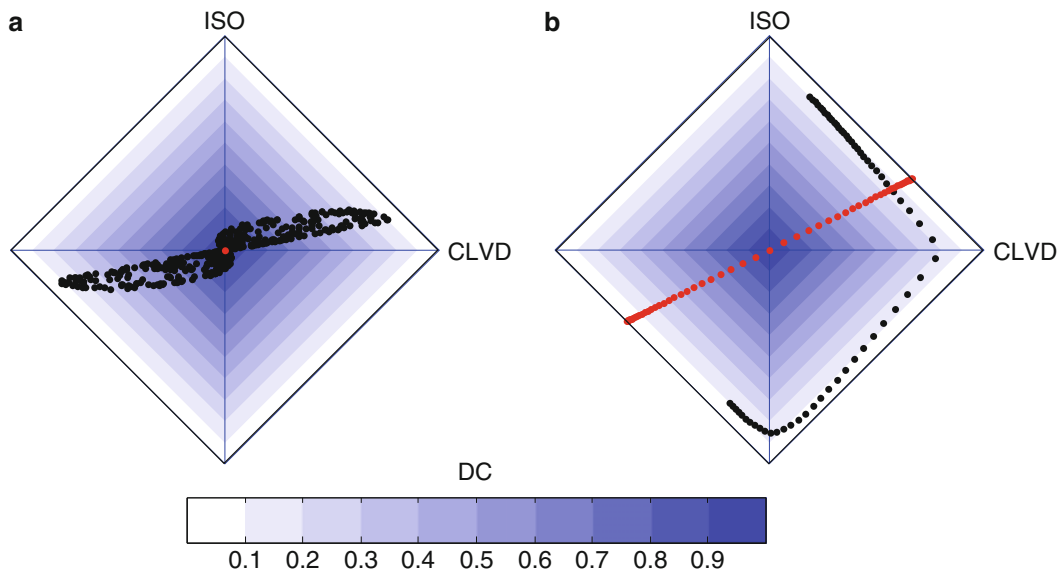


Fig. 10 Diamond source-type plots for the shear (a) and tensile (b) source models in an anisotropic medium. The *black dots* in (a) correspond to 500 moment tensors of shear sources with randomly oriented fault and slip. The *black dots* in (b) correspond to moment tensors of tensile sources with strike = 0° , dip = 20° , and rake = -90° (normal faulting). The slope angle ranges from -90° (pure compressive crack) to $+90^\circ$ (pure tensile crack) in steps of 3° . The *red dots* in (a) and (b) show the corresponding source tensors. The medium is transversely isotropic with the following elastic parameters (in $10^9 \text{ kg m}^{-1} \text{ s}^{-2}$): $c_{11} = 58.81$, $c_{33} = 27.23$, $c_{44} = 13.23$, $c_{66} = 23.54$, and $c_{13} = 23.64$. The medium density is $2,500 \text{ kg/m}^3$. The parameters are taken from Vernik and Liu (1997) and describe the Bazhenov shale (depth of 12,507 ft)

moment tensors of shear faulting (Fig. 10a, black dots) or tensile faulting (Fig. 10b, black dots) may behave in a complicated way. For example, shear faulting in anisotropic media can produce strongly

non-DC moment tensors (Vavryčuk 2005). This prevents a straightforward interpretation of moment tensors in terms of the physical faulting parameters. Therefore, first, the source tensors must be calculated from moment tensors and then interpreted (Fig. 10, red dots). If elastic properties of the medium in the focal zone needed for calculating the source tensors are not known, they can be inverted from the non-DC components of the moment tensors (Vavryčuk 2004, 2011; Vavryčuk et al. 2008). Note that the retrieved medium parameters do not refer to local material properties of the fault, but to the medium surrounding the fault.

Summary

The moment tensor represents equivalent body forces of a seismic source. The forces described by the moment tensor are not the actual forces acting at the source because the moment tensor description assumes elastic behavior of the medium and ignores nonlinear rheology at the focal area. Nevertheless, the moment tensor proved to be a useful quantity and became widely accepted in seismological practice for studying seismic sources. The moment tensor is evaluated for earthquakes on all scales from acoustic emissions to large devastating earthquakes.

In order to understand physical processes at the earthquake source, the moment tensor is commonly decomposed into double-couple (DC), isotropic (ISO), and compensated linear vector dipole (CLVD) components. High percentage of DC indicates a source with shear faulting in isotropic media, and high percentage of ISO indicates an explosive or implosive source. A combination of positive (negative) ISO and CLVD is produced by tensile (compressive) faulting. The type of the source can be visualized using the so-called source-type plots; among them, the diamond CLVD-ISO plot, the Hudson's skewed diamond plot, and the Riedesel-Jordan lune plot are in common use. In anisotropic media, the physical interpretation of the DC, ISO, and CLVD percentages is not straightforward, and the decomposition of the moment tensor must be substituted by that of the source tensor.

Cross-References

- ▶ [Earthquake Mechanism Description and Inversion](#)
- ▶ [Long-Period Moment-Tensor Inversion: The Global CMT Project](#)
- ▶ [Non-Double-Couple Earthquakes](#)
- ▶ [Reliable Moment Tensor Inversion for Regional- to Local-Distance Earthquakes](#)
- ▶ [Regional Moment Tensors Review: An Example from the Euro-Mediterranean Region](#)

References

- Aki K, Richards PG (2002) Quantitative seismology. University Science, Sausalito
- Ben-Zion Y (2003) Appendix 2: key formulas in earthquake seismology. In: Lee WHK, Kanamori H, Jennings PC, Kisslinger C (eds) International handbook of earthquake and engineering seismology, Part B. Academic, London, p 1857
- Bowers D, Hudson JA (1999) Defining the scalar moment of a seismic source with a general moment tensor. Bull Seismol Soc Am 89(5):1390–1394
- Burridge R, Knopoff L (1964) Body force equivalents for seismic dislocations. Bull Seismol Soc Am 54:1875–1888

- Chapman CH, Leaney WS (2012) A new moment-tensor decomposition for seismic events in anisotropic media. *Geophys J Int* 188:343–370
- Dziewonski AM, Chou T-A, Woodhouse JH (1981) Determination of earthquake source parameters from waveform data for studies of global and regional seismicity. *J Geophys Res* 86:2825–2852
- Hudson JA, Pearce RG, Rogers RM (1989) Source type plot for inversion of the moment tensor. *J Geophys Res* 94:765–774
- Jost ML, Herrmann RB (1989) A student's guide to and review of moment tensors. *Seismol Res Lett* 60:37–57
- Julian BR, Miller AD, Foulger GR (1998) Non-double-couple earthquakes 1. Theory *Rev Geophys* 36:525–549
- Kanamori H, Given JW (1981) Use of long-period surface waves for rapid determination of earthquake-source parameters. *Phys Earth Planet In* 27:8–31
- Kawasaki I, Tanimoto T (1981) Radiation patterns of body waves due to the seismic dislocation occurring in an anisotropic source medium. *Bull Seismol Soc Am* 71:37–50
- Knopoff L, Randall MJ (1970) The compensated linear-vector dipole: a possible mechanism for deep earthquakes. *J Geophys Res* 75:4957–4963
- Kuge K, Lay T (1994) Data-dependent non-double-couple components of shallow earthquake source mechanisms: effects of waveform inversion instability. *Geophys Res Lett* 21:9–12
- Miller AD, Foulger GR, Julian BR (1998) Non-double-couple earthquakes 2. Observations. *Rev Geophys* 36:551–568
- Mori J, McKee C (1987) Outward-dipping ring-fault structure at Rabaul caldera as shown by earthquake locations. *Science* 235:193–195
- Riedesel MA, Jordan TH (1989) Display and assessment of seismic moment tensors. *Bull Seismol Soc Am* 79:85–100
- Rudajev V, Šílený J (1985) Seismic events with non-shear components. II. Rockbursts with implosive source component. *Pure Appl Geophys* 123:17–25
- Sipkin SA (1986) Interpretation of non-double-couple earthquake mechanisms derived from moment tensor inversion. *J Geophys Res* 91:531–547
- Tape W, Tape C (2012) A geometric comparison of source-type plots for moment tensors. *Geophys J Int* 190:499–510
- Vavryčuk V (2001) Inversion for parameters of tensile earthquakes. *J Geophys Res* 106(B8):16.339–16.355. doi:10.1029/2001JB000372
- Vavryčuk V (2004) Inversion for anisotropy from non-double-couple components of moment tensors. *J Geophys Res* 109:B07306. doi:10.1029/2003JB002926
- Vavryčuk V (2005) Focal mechanisms in anisotropic media. *Geophys J Int* 161:334–346. doi:10.1111/j.1365-246X.2005.02585.x
- Vavryčuk V (2011) Tensile earthquakes: theory, modeling, and inversion. *J Geophys Res* 116:B12320. doi:10.1029/2011JB008770
- Vavryčuk V (2015) Moment tensor decompositions revisited. *J Seismol* 19:231–252. doi:10.1007/s10950-014-9463-y
- Vavryčuk V, Bohnhoff M, Jechumtálová Z, Kolář P, Šílený J (2008) Non-double-couple mechanisms of micro-earthquakes induced during the 2000 injection experiment at the KTB site, Germany: a result of tensile faulting or anisotropy of a rock? *Tectonophysics* 456:74–93. doi:10.1016/j.tecto.2007.08.019
- Vernik L, Liu X (1997) Velocity anisotropy in shales: a petrological study. *Geophysics* 62:521–532
- Wallace TC (1985) A reexamination of the moment tensor solutions of the 1980 Mammoth Lakes earthquakes. *J Geophys Res* 90:11,171–11,176